

## Femtosecond fiber Bragg grating fabrication with adaptive optics aberration compensation

PATRICK S. SALTER,<sup>1,2</sup>  MATTHEW J. WOOLLEY,<sup>1</sup>  STEPHEN M. MORRIS,<sup>1</sup> MARTIN J. BOOTH,<sup>1</sup>   
AND JULIAN A. J. FELS<sup>1,3</sup> 

<sup>1</sup>Department of Engineering Science, University of Oxford, Parks Road, Oxford OX1 3PJ, UK

<sup>2</sup>e-mail: patrick.salter@eng.ox.ac.uk

<sup>3</sup>e-mail: julian.fels@eng.ox.ac.uk

Received 22 August 2018; revised 6 November 2018; accepted 7 November 2018; posted 9 November 2018 (Doc. ID 342972); published 7 December 2018

We present fiber Bragg gratings (FBGs) fabricated using adaptive optics aberration compensation for the first time to the best of our knowledge. The FBGs are fabricated with a femtosecond laser by the point-by-point method using an air-based objective lens, removing the requirement for immersion oil or ferrules. We demonstrate a general phase correction strategy that can be used for accurate fabrication at any point in the fiber cross-section. We also demonstrate a beam-shaping approach that nullifies the aberration when focused inside a central fiber core. Both strategies give results which are in excellent agreement with coupled-mode theory. An extremely low wavelength polarization sensitivity of 4 pm is reported.

Published by The Optical Society under the terms of the [Creative Commons Attribution 4.0 License](https://creativecommons.org/licenses/by/4.0/). Further distribution of this work must maintain attribution to the author(s) and the published article's title, journal citation, and DOI.

<https://doi.org/10.1364/OL.43.005993>

Fiber Bragg gratings (FBGs) have become ubiquitous for sensing parameters such as strain, temperature, and pressure in remote and extreme environments [1]. Currently deployed FBGs are typically fabricated by exposing photosensitive optical fibers to ultra-violet (UV) radiation by interfering two beams [2] or using a phase mask [3]. Femtosecond laser written FBGs, on the other hand, use an ultrafast laser with sub-picosecond pulse duration, providing an inherent three-dimensional resolution to the fabrication, to directly modify the glass structure inside the fiber core. While the quality of femtosecond FBGs is typically inferior to their UV counterparts, they may be written in standard silica single mode fiber (SMF) without pre-processing such as hydrogenation, reducing time and cost. Furthermore, they may withstand temperatures of up to 1000°C [4] without post-treatment, such as curing or regeneration, which can be detrimental to mechanical integrity.

The cylindrical geometry of an optical fiber leads to aberration when focusing inside with air-based lenses, as illustrated in

Fig. 1(a). Rays with a component parallel to the fiber axis are refracted at the fiber interface, while those that are purely perpendicular remain unaffected, leading to focal splitting and distortion. This is detrimental as high precision is required in the fabrication process to enable short grating pitches of  $\sim 1 \mu\text{m}$ . Various attempts have been made to mitigate aberration, such as immersing the fiber in index matching oil [5–8] or placing the fiber in a ferrule [9], but these are not well suited for volume manufacturing. Recently, the aberration has been corrected by using a pair of static cylindrical lenses [10]. Unfortunately, there is a limit to the correction possible with static lenses and the devices exhibited strong polarization dependency of 2.2 dB in transmission and 60 pm in wavelength. While adaptive elements, such as a deformable mirror [11] and a spatial light modulator (SLM) [12], have been used previously to adjust the Bragg wavelength using a phase mask technique, in this Letter, we employ such an element to correct

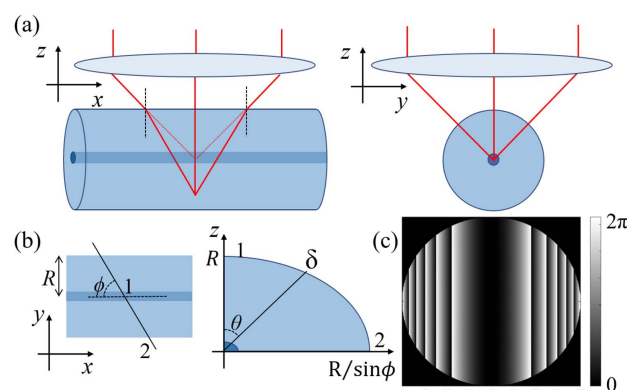


**Fig. 1.** Diagrammatic illustration of the aberration incurred when focusing inside an optical fiber. (a) Ray paths of writing beam for axial plane ( $z$ - $x$ ) and radial plane ( $z$ - $y$ ) of optical fiber. Refraction at the fiber interface causes a focal splitting between components of rays propagating parallel and perpendicular to the fiber axis. (b) By considering a cross-section through the fiber at an angle  $\phi$  to the fiber axis, it is possible to determine the pupil phase aberration that needs to be corrected to focus inside the fiber core, as shown in (c) for a typical SMF with a 0.5 NA air objective.

for optical aberration in FBG fabrication for the first time to the best of our knowledge. Two different techniques, aberration correction and beam-shaping, are used to enable high quality FBGs with good spectral response and low polarization sensitivity, without the use of ferrules or oil immersion optics.

The task of aberration correction is greatly simplified if it is possible to accurately predict the phase aberration induced during focusing, as is the case here since both the geometry and refractive index of the fiber are known. Thus, following the method described in Ref. [13], we calculate the additional phase delay  $\psi$  for rays focused at the fiber core due to the presence of the fiber as  $\psi = 2\pi\delta\Delta n/\lambda$ , where  $\lambda$  is the wavelength of the light,  $\Delta n$  is the difference in refractive indices between fiber and air, and  $\delta$  is the physical path length inside the fiber as shown in Fig. 1(b). Considering the intersection of the fiber and the  $x$ - $y$  plane at angle  $\phi$  to the fiber axis, the fiber interface traces out an ellipse [Fig. 1(b)]. We employ the sine condition,  $\sin \theta = \rho \text{NA}$ , to map a ray at an angle,  $\theta$ , to the optic axis to a normalized radius  $\rho$  in the pupil plane of the objective with numerical aperture NA. Simple geometry gives the phase aberration as

$$\psi = \frac{2\pi\Delta nR}{\lambda\sqrt{1-\rho^2\text{NA}^2\cos^2\phi}}, \quad (1)$$

where  $R$  is the fiber radius. The pupil phase predicted in Eq. (1) is plotted in Fig. 1(c) for a 0.5 NA air objective focused to the core of SMF with diameter  $2R = 125 \mu\text{m}$ . By approximating to the case of a low NA objective lens ( $\text{NA} \lesssim 0.5$ ), Eq. (1) can be expanded as

$$\begin{aligned} \psi &\cong \frac{2\pi\Delta nR}{\lambda} \left( 1 + \frac{\rho^2\text{NA}^2}{4} + \frac{\rho^2\text{NA}^2 \cos 2\phi}{4} \right) \\ &= aZ_0^0 + bZ_2^0 + cZ_2^2, \end{aligned} \quad (2)$$

which can be decomposed exactly into  $Z_0^0, Z_2^0, Z_2^2$  corresponding to the Zernike modes for piston, defocus, and primary astigmatism, respectively, with coefficients  $a$ ,  $b$ , and  $c$ . While Eqs. (1) and (2) describe the aberration focusing into the center of the fiber, similar expressions can be obtained for other positions within the fiber cross-section for the fabrication of more complex configurations. The “aberration correction” technique uses a dynamic optical element to pre-distort the beam with the phase  $-\psi$  to correct for the phase aberration and achieve a tight focus in the fiber.

An alternative way of compensating for aberration, when writing in the central axis of the fiber, is to use a “beam-shaping” technique. From the symmetry of the phase pattern in Fig. 1(c), it can be seen that it is possible to negate the effect of the phase aberration by reducing the dimensionality in the pupil illumination. For example, a narrow-slit illumination along the  $y$ -axis as indicated in Fig. 2(a) (Slit 1) would see a uniform phase distribution. However, this reduction of the NA in the focusing lens along the  $x$ -direction would lead to a spread of the focal intensity along the fiber core [Fig. 2(c), Slit 1], which would be undesirable for the fabrication of tight pitch gratings. Alternatively, if there is a slit illumination oriented along the  $x$ -direction [Slit 2 in Fig. 2(a)], the phase distribution is not uniform, but in the low NA limit can be approximated as quadratic, as seen from Eq. (2) and plotted in Fig. 2(b). A quadratic phase in this regime corresponds to simply refocusing the optical system, which can be readily achieved using a translation stage. An added benefit of

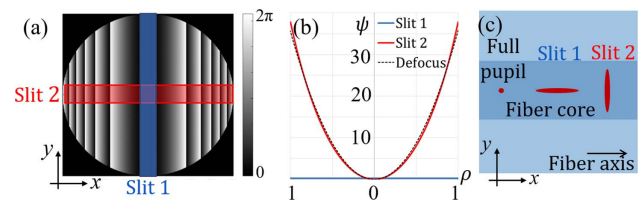


**Fig. 2.** Illumination of the objective lens pupil with a slit intensity distribution as shown in (a) reduces the dimensionality and can effectively remove the phase aberration. (b) The phase profile plotted along each of the slits indicated in (a) as well as the theoretical defocus. (c) Schematic of the focal intensity distribution in the fiber core with different illumination profiles of the objective lens.

the slit illumination in this orientation is that the focal intensity maintains resolution parallel to the fiber axis but is spread perpendicular to the axis [Fig. 2(c), Slit 2]. Therefore, the structural modification is more symmetric about the fiber axis and covers a larger extent of the fiber core, in an analogous fashion to slit beam shaping for the fabrication of symmetric micro-channels [14], waveguides [15] and indeed FBGs in  $D$ -shaped fiber [16]. We would thus expect that the slit beam shaping in this scenario not only removes the need for aberration correction but additionally should reduce polarization sensitivity and increase the coupling coefficient of the grating.

Both the aberration correction technique and the beam-shaping technique are demonstrated in this work using femto-second laser fabrication inside the core of SMF. The laser beam from a regeneratively amplified Ti:Sapphire laser (100 Hz, 100 fs,  $\lambda = 790 \text{ nm}$ ) was expanded and directed onto a phase-only reflective liquid crystal SLM (Hamamatsu X10468-02). The SLM was imaged in a  $4f$  configuration onto the pupil plane of a Zeiss  $20 \times 0.5 \text{ NA}$  air objective. The fiber was mounted on a 3D precision translation stage (Aerotech ABL10100, ANT95-3) and moved relative to the laser focus at a speed of  $0.106 \text{ mm/s}$  to create a point-by-point FBG with a period of  $1.06 \mu\text{m}$ .

To implement the aberration correction technique, phase patterns corresponding to  $-\psi$  from Eq. (1) were displayed on the SLM. For the beam-shaping technique, a blazed grating was displayed on the SLM and a beam block was inserted into the Fourier plane, positioned such that it only passed the first diffracted order. Thus, by selectively patterning the SLM with the grating, it was possible to generate adaptive strip illumination of the objective, as described in Ref. [17]. An effective slit width of  $800 \mu\text{m}$  at the objective was found to be optimum in terms of negating the aberration, spreading the focal intensity and allowing reasonable throughput. In principle, a physical slit could be used in place of the SLM. However, the SLM has the advantage that it can be imaged exactly on the pupil plane of the objective, whereas there is a limit to how close a slit could be positioned. The SLM also has the benefit of allowing it to be adaptively trimmed to a particular fiber and grating design.

Figure 3 shows microscope images for structures fabricated inside SMF using the aberration correction technique. In Fig. 3(a), the correction is applied to the SLM as described by Eq. (1). A pulse energy of  $140 \text{ nJ}$ , measured before the objective lens, was required to fabricate single points in the fiber core, with dimensions  $0.7 \mu\text{m} \times 2.2 \mu\text{m}$  consistent with the diffraction limit. When the phase correction was removed from

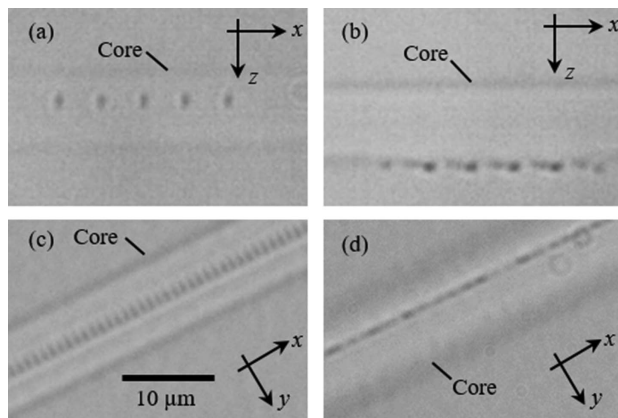


**Fig. 3.** Microscope images of structures fabricated inside SMF. A series of 5 points, each fabricated by a single pulse at 5  $\mu\text{m}$  spacing with (a) and without (b) aberration correction. The laser was incident along the  $z$  direction. FBGs fabricated with (c) and without (d) correction.

the SLM, the pulse energy needed to be raised to 500 nJ to fabricate single points due to the focal distortion associated with the aberration. Each point was extended along the axis of the fiber to a dimension of 3.7  $\mu\text{m}$ , as shown in Fig. 3(b). In addition, the focal distortion shifted the structure outside of the core, even though there was no refocusing of the optical system. When writing FBGs, the aberration correction maintained sufficient resolution to accurately fabricate structures on a 1  $\mu\text{m}$  pitch, as shown in Fig. 3(c), where we additionally note that the pulse energy used was slightly elevated above those appropriate for device fabrication in order to improve visualization for the images. Without aberration correction, Fig. 3(d), any discernible structure was lost from the grating due to the distortion in the laser focus.

Second order FBGs were written in standard SMF (9/125  $\mu\text{m}$ , G.652D), and the primary coating was removed. The grating length was 3 mm and various pulse energies were used to obtain different magnitudes of refractive index change and hence coupling coefficient,  $\kappa$ . The FBGs were unapodized, with uniform  $\kappa$  over the whole length and an abrupt transition at each end. This results in side-lobes that enable comparison with the theoretical response and an assessment of the grating uniformity by their symmetry and relative side-lobe levels. For use in sensors, the side-lobes can be removed by apodization such that there is a smooth transition in grating strength at the grating edges.

The spectral performance was measured using a tunable laser (Agilent 81642A) in conjunction with an optical power meter (Newport 1830-C). To measure the reflection spectrum, a 3 dB fiber coupler was used with the tunable laser and optical power meter on each of the input ports and the FBG on one output port. The unused output port and the other end of the FBG were optically terminated and APC connectors were used for all connections. The reflection spectra were fitted to the coupled-mode solution [18] to enable the coupling coefficients to be determined. Figure 4 shows the reflection spectrum and fitted coupled-mode solution for 3 mm FBGs, written using aberration correction [Fig. 4(a)] and beam-shaping [Fig. 4(b)], for coupling coefficients of 1, 2, and 3  $\text{cm}^{-1}$ . The respective pulse energies are 48, 56, and 65 nJ for aberration correction and 297, 316, and 357 nJ for beam-shaping [the spread in focal

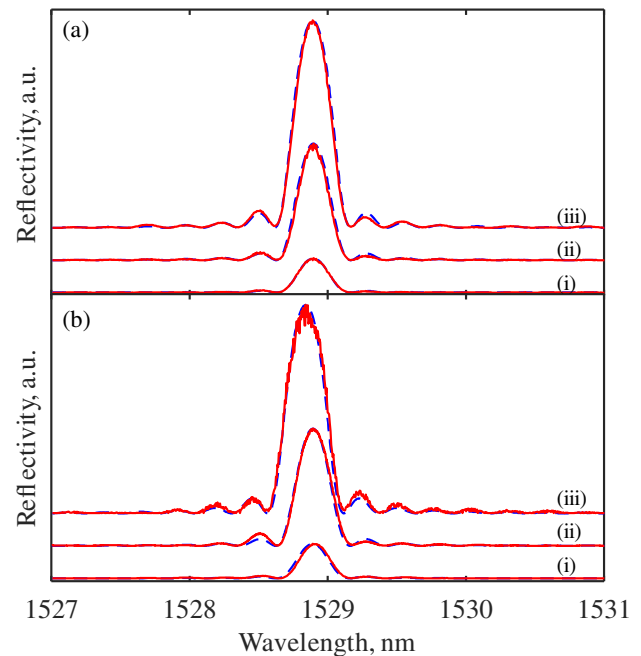


**Fig. 4.** Measured and theoretical reflection spectra for fabricated FBGs with 3 mm length, (— red) experimental measurement, (--- blue) fit to coupled-mode theory, (a) using aberration correction (b) using beam-shaping, for coupling coefficient,  $\kappa$  and reflectivity  $R$ , (i)  $\kappa = 1 \text{ cm}^{-1}$ ,  $R = 8.5\%$ , (ii)  $\kappa = 2 \text{ cm}^{-1}$ ,  $R = 28.8\%$  and (iii)  $\kappa = 3 \text{ cm}^{-1}$ ,  $R = 51.3\%$ . See Data File 1 for the underlying data.

intensity for the beam shaping method, Fig. 2(c), necessitates higher pulse energy to maintain an equivalent fluence at focus]. There is exceptionally good agreement between the experimentally measured reflectivity and the theoretical reflectivity in all cases. The strong correlation between theory and experiment indicates neither compensation technique has compromised the FBG uniformity.

Optical aberrations can cause the writing laser focus to become distorted in the  $z$ - $y$  plane, such that the index change is not circularly symmetric, resulting in polarization dependence. The polarization sensitivity of the FBGs written with aberration compensation were analyzed in transmission. The tunable laser was connected to a polarization controller, followed by the FBG and then the optical power meter. The worst-case polarization states were explored by first positioning the laser wavelength on the Bragg peak and adjusting for minimum and maximum power to look for changes in transmission. This was followed by positioning the laser wavelength on the side of the Bragg peak to look for changes in Bragg wavelength. A number of scans across wavelengths were also made to ensure the polarization sensitivity was fully explored.

Figure 5 shows the two extreme polarization states for two FBGs. Figure 5(a) shows an FBG fabricated using the aberration technique and Fig. 5(b) shows an FBG written using the beam-shaping technique. The data in Fig. 5 shows the reflection polarization sensitivity to be 0.14 dB and 0.44 dB for FBGs fabricated using the aberration correction technique and the beam-shaping technique, respectively. However, it is the wavelength polarization sensitivity which is of most interest as this can have a direct consequence on the performance of



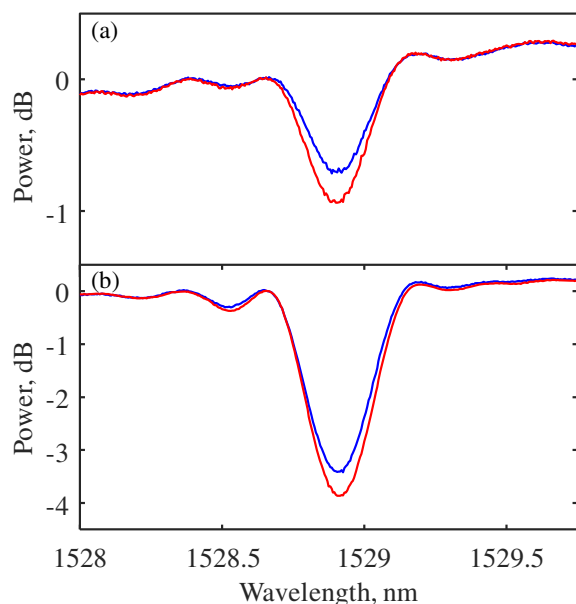


**Fig. 5.** Measured polarization sensitivity of FBGs, fabricated with (a) the aberration correction technique and (b) the beam-shaping technique. The two lines represent the two extreme polarization states. See [Data File 2](#) for the underlying data.

FBG sensors. The wavelength polarization sensitivity was determined by applying a digital 7-point moving average filter with Gaussian coefficients and determining the minimum Bragg reflection. It was found to be only 8 pm for the FBG with aberration correction and only 4 pm for the FBG with beam-shaping. This latter figure is more than an order of magnitude better than the 60 pm reported in Ref. [10], though this was for a stronger FBG. The beam-shaping technique gives slightly better performance than the aberration correction technique.

Both compensation techniques are applicable for fabrication in the core of coated fiber with air-based optics. However, the aberration correction technique gives greater flexibility because by adjusting the phase correction applied to the SLM, it could be used to write off-center in the fiber. It may therefore be used to write FBGs in multicore fibers [19] and for other novel devices such as waveguide couplers [20]. Furthermore, the phase correction could be adjusted to compensate for internal interfaces in specialty fibers such as photonic crystal fibers [21] and air-hole fibers [22], where the aberration cannot be mitigated by immersion oil or ferrules.

In conclusion, we have demonstrated a new concept for writing high quality femtosecond FBGs using air-based lenses. As a result, the fabrication process is far better suited to mass production of femtosecond FBGs than oil immersion or ferrules. The aberration present during writing is compensated by applying a modification to the beam wave front using a SLM. Two alternative types of compensation have been applied: aberration correction and beam-shaping. Both compensation

techniques gave reflectivity spectra which had excellent correlation to coupled-mode theory. The aberration correction and beam-shaping techniques resulted in the fabrication of FBGs with very low polarization sensitivities of 8 pm and 4 pm, respectively. These techniques will therefore allow volume manufacture of FBGs, which simultaneously combine high performance with environmental robustness. Furthermore, the enhanced precision afforded may open up new device possibilities.

**Funding.** Engineering and Physical Sciences Research Council (EPSRC) (EP/M017923/1, EP/R004803/1).

**Acknowledgment.** We thank Professor Dominic C. O'Brien for use of the optical fiber test equipment.

## REFERENCES

- S. J. Mihailov, *Sensors* **12**, 1898 (2012).
- G. Meltz, W. W. Morey, and W. H. Glenn, *Opt. Lett.* **14**, 823 (1989).
- K. O. Hill, B. Malo, F. Bilodeau, D. C. Johnson, and J. Albert, *Appl. Phys. Lett.* **62**, 1035 (1993).
- C. W. Smelser, S. J. Mihailov, and D. Grobnc, *Opt. Express* **13**, 5377 (2005).
- Y. Lai, K. Zhou, K. Sugden, and I. Bennion, *Opt. Express* **15**, 18318 (2007).
- K. Zhou, M. Dubov, C. Mou, L. Zhang, V. K. Mezentssev, and I. Bennion, *IEEE Photon. Technol. Lett.* **22**, 1190 (2010).
- R. J. Williams, R. G. Krämer, S. Nolte, and M. J. Withford, *Opt. Lett.* **38**, 1918 (2013).
- E. Ertoer, M. Haque, J. Li, and P. R. Herman, *Opt. Express* **26**, 9323 (2018).
- G. D. Marshall, R. J. Williams, N. Jovanovic, M. J. Steel, and M. J. Withford, *Opt. Express* **18**, 19844 (2010).
- Y. Chen, Y. Lai, and M. W. O. Cheong, *Appl. Opt.* **55**, 5575 (2016).
- T. A. Goebel, C. Voigtländer, R. G. Krämer, D. Richter, M. Heck, M. P. Siems, C. Matzdorf, C. Reinlein, M. Appelfelder, T. Schreiber, J. U. Thomas, A. Tünnermann, and S. Nolte, *Opt. Lett.* **42**, 4215 (2017).
- C. Voigtländer, R. G. Krämer, T. A. Goebel, D. Richter, and S. Nolte, *Opt. Lett.* **41**, 17 (2016).
- M. Schwertner, M. J. Booth, and T. Wilson, *J. Microsc.* **215**, 271 (2004).
- Y. Cheng, K. Sugioka, K. Midorikawa, M. Masuda, K. Toyoda, M. Kawachi, and K. Shihoyama, *Opt. Lett.* **28**, 55 (2003).
- M. Ams, G. D. Marshall, D. J. Spence, and M. J. Withford, *Opt. Express* **13**, 5676 (2005).
- B. Malo, K. O. Hill, F. Bilodeau, D. C. Johnson, and J. Albert, *Electron. Lett.* **29**, 1668 (1993).
- P. S. Salter, A. Jesacher, J. B. Spring, B. J. Metcalf, N. Thomas-Peter, R. D. Simmonds, N. K. Langford, I. A. Walmsley, and M. J. Booth, *Opt. Lett.* **37**, 470 (2012).
- T. Erdogan, *J. Lightwave Technol.* **15**, 1277 (1997).
- A. Donko, M. Beresna, Y. Jung, J. Hayes, and D. J. Richardson, *Opt. Express* **26**, 2039 (2018).
- K. K. C. Lee, A. Mariampillai, M. Haque, B. A. Standish, V. X. D. Yang, and P. R. Herman, *Opt. Express* **21**, 24076 (2013).
- J. C. Knight, T. A. Birks, P. St.J. Russell, and D. M. Atkin, *Opt. Lett.* **21**, 1547 (1996).
- C. M. Jewart, Q. Wang, J. Canning, D. Grobnc, S. J. Mihailov, and K. P. Chen, *Opt. Lett.* **35**, 1443 (2010).